Fermilab FERMILAB-Conf-01/304-E November 2001

Benchmarking Residual Dose Rates in a NuMI-like Environment*

I. Rakhno†, N. Mokhov, A. Elwyn, and N. Grossman
Fermi National Accelerator Laboratory, Batavia, Illinois 60510-0500, USA

M. Huhtinen
CERN, Geneva, CH-1211, Switzerland

and

L. Nicolas
University of Orsay, Paris, France

Abstract – *Activation of various structural and shielding materials is an important issue for many applications. A model developed recently to calculate residual activity of arbitrary composite materials for arbitrary irradiation and cooling times is presented in the paper. Measurements have been performed at the Fermi National Accelerator Laboratory using a 120 GeV proton beam to study induced radioactivation of materials used for beam line components and shielding. The calculated residual dose rates for the samples studied behind the target and outside of the thick shielding are presented and compared with the measured ones. Effects of energy spectra, sample material and dimensions, their distance from the shielding, and gaps between the shielding modules and walls as well as between the modules themselves were studied in detail.*

I. INTRODUCTION

An important issue regarding the radiation environment in the NuMI-MINOS neutrino experiment, currently under construction at Fermi National Accelerator Laboratory (FNAL),[1] is induced radioactivation of the beam line components and shielding materials. This arises from irradiation by hadrons that are generated in the target bombarded by an 120 GeV proton beam. The MARS Monte Carlo code[2] is used to predict and analyse prompt and residual radiation in such an environment. The prediction for the latter is based on a new algorithm described in this paper. To understand the properties of the residual radiation and benchmark the newly developed code modules, measurements were performed both in the vault area and at a location outside the steel shielding at the antiproton (AP0) target area, which is thought to be a close representation of the NuMI target area. All the details of the AP0 enclosure (in-vault and outside the shielding) and the appropriate beam line components were built into the MARS calculation model and detailed simulations were performed. Calculated residual dose rates and neutron spectra are compared with the data showing general good agreement.

* Work supported by the Universities Research Association, Inc., under contract DE-AC02-76CH03000 with the U.S. Department of Energy.

† rakhno@fnal.gov

II. EXPERIMENTAL SETUP

A MARS model of the experimental setup is shown in Fig. 1. Residual activation exposure rates were measured for five small cylindrical and rectangular samples of iron, steel, aluminum, and concrete, which were obtained from materials that will be used in the NuMI construction. Composition of the samples is described in Table I. The samples were placed both within the vault area (just downstream of the antiproton production target) and at a location outside of the steel shielding at AP0. Further, thin activation foils of Al, In, and Au as well as Au covered with Cd were mounted on a disk and placed at both locations. The neutron spectrum at the in-vault location was unfolded from measured foil activities by use of response functions determined from known cross section data with the unfolding codes BUNKI and LOUHI.[3] The samples within the vault were irradiated for a total of 38 hours by the radiation arising from the bombardment of the target by about 1.3×10^{17} 120 GeV protons from the Main Injector, and then removed to a low background area for counting; those outside of the shielded vault area were irradiated on and off for about four months with a total of approximately 3.6×10^{18} protons incident on the in-vault target. Background corrected exposure rates of the samples were determined by use of both Geiger-Müller (GM) and NaI scintillator based survey instruments.

III. CALCULATION MODEL

III.A. Model for residual dose rate estimation

While most of the values predicted with modern Monte Carlo codes for high energy accelerator environments can be obtained with a rather high accuracy, residual dose rates remain less reliable. Uncertainty up to a factor of three can be considered as typical. This is because of the complicated na-

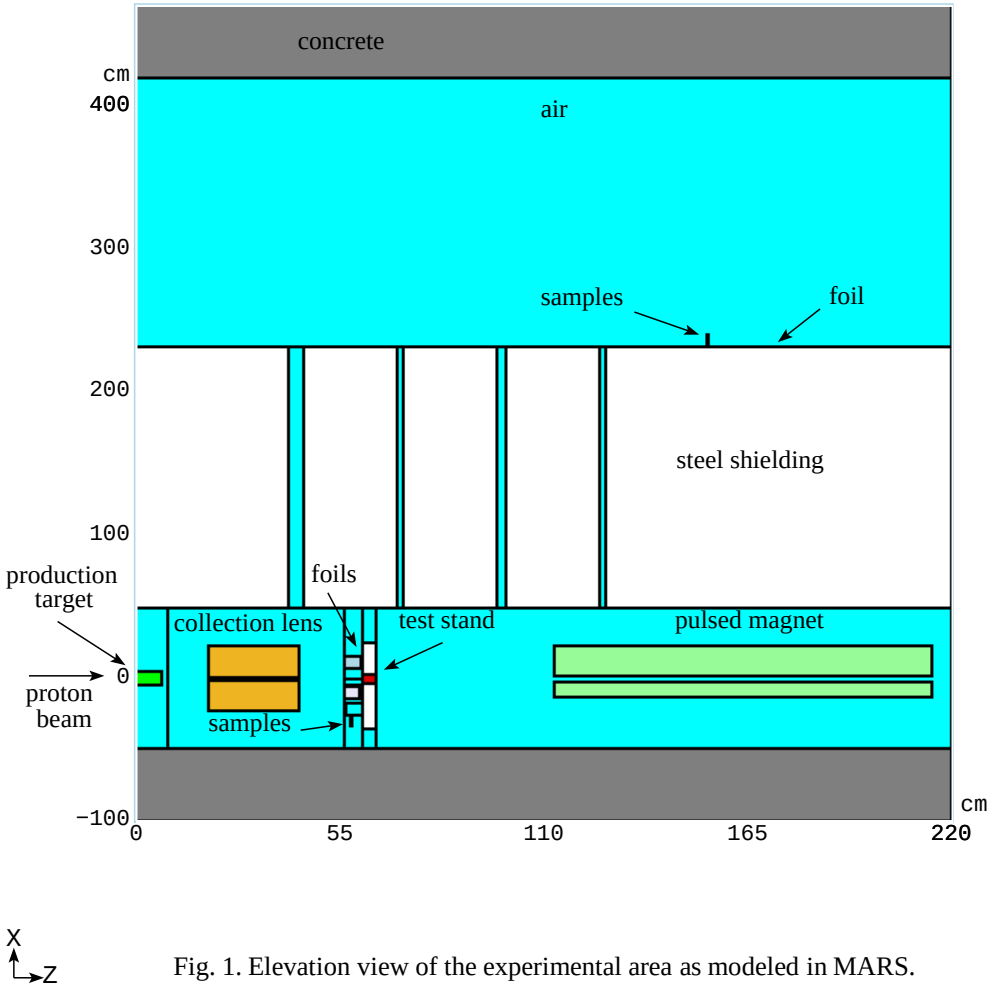

Fig. 1. Elevation view of the experimental area as modeled in MARS.

TABLE I. Composition of the samples investigated (weight %)

Sample	Nuclide (or natural mixture)													
	^{1}H	^{12}C	^{16}O	^{23}Na	Mg	^{27}Al	Si	S	K	Ca	^{55}Mn	Fe	Ni	Cu
1 (Aluminum)						100								
2 (Iron)		0.1					0.1				0.4	98.2	1.0	0.2
3 (1018 Steel)		0.2									0.9	98.9		
4 (Concrete[a])	0.8	7.3	51.76	0.07	6.5	0.5	10.1	0.2	0.07	21.1		1.6		
5 (A500 Steel)		0.3										99.5		0.2

[a]Precise composition of the concrete sample is not presently known. This Table shows the reference composition used.

ture of this phenomenon and its high sensitivity to the composition of irradiated materials. In principle, a multi-step approach based on a hadron transport code (e.g., MARS or FLUKA[4]) coupled to a nuclide transmutation inventory code (CINDER[5] or DeTra[6]), would provide the most reliable solution of activation problems – provided the hadron code is able to deliver adequate residual nuclide yields from high-energy interactions. In practice, however, one often uses an approach based on so-called ω-factors that convert the star density (a density of inelastic nuclear interactions above 50 MeV) to a contact residual dose rate, independent (often) of the material for the fixed set of irradiation (T_i) and cooling (T_c) times (typically T_i=30 days, T_c=1 day). As can be seen,[7] this model is a rather crude approach to real situations. In particular, it has been shown [8] that when defining ω-factors a 20 MeV star threshold should be used instead of the historical 50 MeV.

New modules have been developed for the current version of the MARS14 code[2] to substantially improve the reliability of the ω-factor based predictions of residual dose rates in arbitrary composite materials for arbitrary irradiation and cooling times. The algorithm distinguishes three major energy groups responsible for radionuclide production: (1) above 20 MeV, (2) 1 to 20 MeV, and (3) below 0.5 eV. The energy groups were chosen to consider separately the most important nuclear reactions responsible for induced radioactivation in the regions: high energy inelastic interactions (mostly spallation reactions), threshold reactions $(n,2n)$, (n,p) *etc*, and (n,γ) reactions, respectively. Neutrons in the energy region from 0.5 eV to 1 MeV do not produce a significant number of radionuclides. Detailed FLUKA calculations[4] were performed for cascades induced by energetic hadrons in cylindrical samples of 17 elements: C, O, Na, Mg, Al, Si, K, Ca, Cr, Fe, Ni, Cu, Nb, Ag, Ba, W, Pb. Creation of the residual nuclides close to the cascade core was simulated. The decay chains of the created radionuclides were followed with the DeTra code in order to determine the emission rates of de-excitation photons for 12 hours$< T_i <$20 years and 1 sec$< T_c <$20 years. Corresponding dose rates on the outer surfaces were calculated from photon fluxes and related to the star density above 20 MeV (first group), and neutron fluxes in two other energy groups. Results were collected in the database. This method essentially applies the optimum method of activation prediction described above to derive a set of material and time dependent ω-factors which are easy to use in a routine cascade simulation and should provide far better accuracy than the old approach.

A sophisticated interpolation algorithm, linked to this database, was created and implemented into the MARS14 code. As an example, numerical values of the ω-factors at typical conditions (30 days irradiation and 1 day cooling) are presented in Fig. 2.

According to the model described, the contact residual dose rates are calculated in MARS on the surface of irradiated samples with linear dimensions of at least 0.5 λ_{in}, where λ_{in} is the nuclear interaction length. Such an approach has the advantage of using geometry- and dimension-independent contact residual dose rates. However, when considering small samples, one must take into account geometry factors to perform conversion of calculated contact dose rates from the large default samples to realistic ones. The factors for the samples under investigation (see Table I) were determined by means of the MCNP[9] code according to the following two-step procedure. First, the dose rate was calculated on the surface of a large sample of a given material at a given specific activity. Second, the dose rate was calculated on the surface of a given realistic small sample of the same material and at the same specific activity. The geometry conversion factor for the given small sample was defined as the ratio of the contact dose rate calculated at the first step to that calculated at the second step. Afterwards all the contact dose rates calculated with the MARS code for the large sample are divided by the factor obtained thus giving rise to results for the small sample of the same material. Isotropic and monoenergetic 1 MeV gammas with uniform spatial distribution were used in these calculations to simulate a residual activity source (see section III.C.). The dimensions and calculated geometry conversion factors for the samples under investigation are presented in Table II.

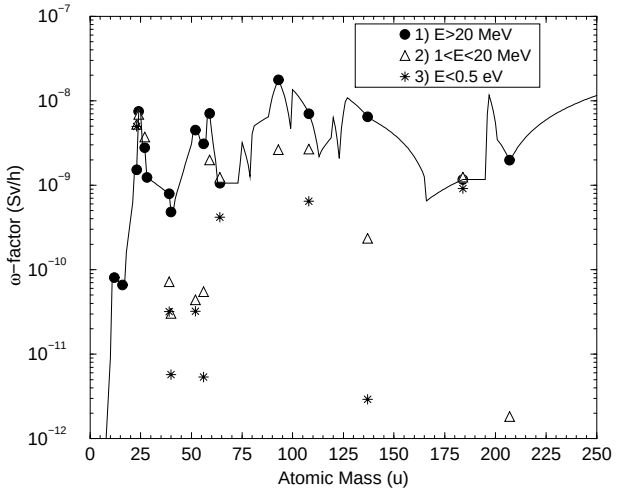

Fig. 2. Example of ω-factor dependence on mass of a target nucleus for three energy groups and T_i=30 days and T_c=1 day. Normalization is per $star/cm^3/s$ for $E > 20$ MeV, and per $neutron/cm^2/s$ for the other groups. The symbols represent the FLUKA results of this study and the curve is an interpolation of the new results and those of a previous study[7] for the high energy group.

TABLE II. Calculated geometry conversion factors for the samples under investigation.

Sample	Dimensions	Geometry factor
1 (Aluminum)	R=1.27 cm, H=7.65 cm	6.3
2 (Iron)	R=1.35 cm, H=3.85 cm	2.7
3 (1018 Steel)	R=1.27 cm, H=7.65 cm	2.4
4[a] (Concrete)	R=1.27 cm, H=1.60 cm	11
4[b] (Concrete)	R=1.27 cm, H=0.30 cm	21
5 (A500 Steel)	5cm X 2.5cm X 1.15cm	2.8

[a] Sample behind the target.
[b] Sample above the shielding.

III.B. Coupling MARS with MCNP

In the current MARS version[2] the MCNP code[9] is invoked whenever a low-energy (under 14.5 MeV) neutron collision with matter is simulated. When considering a problem with dominating low-energy neutron radiation, a standalone MCNP modeling of neutron transport in matter can have some advantages. A new option for MARS-to-MCNP

coupling was developed recently.[a] Namely, when modeling neutron transport with the MARS code, instead of low-energy neutron tracking, one can generate a file containing all the necessary phase-space coordinates for all the neutrons slowed-down to energies under 14.5 MeV. The file can be used as a neutron source for subsequent standalone MCNP modeling. This mode is used in the current study to calculate neutron fluxes over the samples above the shielding, with appropriate variance reduction techniques built in MCNP. Residual dose rates for the samples were determined using the fluxes and database of the ω-factors built in MARS (see Fig. 2 and section IV.B.).

It will be shown in the following sections that in the in-vault region at the location of the thin foils the calculated neutron spectrum has a low-energy part (under 20 MeV) that contains approximately 90% of all neutrons. As for above the vault shielding, the calculated low-energy part amounts to about 99.9%. This is a justification of the importance of contribution from the second and third energy groups (1 to 20 MeV and below 0.5 eV, respectively) for correct prediction of residual activity and, therefore, the option for low-energy neutron transport used in the calculations described.

III.C. Dose rate attenuation factors

Measurement of the residual dose rate for a sample can be performed both on contact and at a distance. To have a simple and easy-to-use relationship when comparing measured or calculated contact dose rate with that at a distance (typically at 30.5 cm), calculations with the MCNP code[9] have been performed. Two types of samples were taken into consideration; namely, cylinders and parallelepipeds of the same radii (1.27 cm) and thicknesses (2.54 cm), respectively, but with other dimensions being different. Several material compositions were used in the study. Residual activity of the samples was simulated by means of gammas born with isotropic angular distribution and spatially uniform over a sample volume. Monoenergetic 1-MeV gammas were considered; this adequately represents the average energy of gammas emitted from different irradiated concrete or steel samples.

Both contact (D_1) and remote (D_2) dose rates were determined as average values over surface segments with linear dimension equal to one inch. One of the segments was located on a surface of a sample under consideration, the second one at different distances d from the sample. The ANSI/ANS-6.1.1-1977 table[9] was used to convert the calculated photon fluxes over the segments to dose rates. The dose rate attenuation factor for a given distance from a sample surface $D(d)$ was determined as the ratio of the calculated dose rates for the two segments at that distance, $D(d) = D_1/D_2(d)$. The calculated factors were fitted as $D(d) = d^{\alpha}$ using χ^2 criterion, where α is the fitted parameter. Typical behaviour of the attenuation factors is presented in Fig. 3.

To estimate influence of the energy spectrum used for gammas, similar calculations have been performed for a steel cylindrical sample 1.27 cm in radius and 2.54 cm in height (see Fig. 3) with energy spectrum of gammas emitted from an iron infinite cylinder 15 cm in radius, irradiated with 100 GeV protons for 30 days and cooled for 30 days. Average energy in such a spectrum equals to 796 keV. Fitted α parameter in this case equals to 1.941 which is very close to the parameter obtained for monoenergetic 1 MeV gammas, namely 1.936 (see Fig. 3). The difference in α values gives rise to the maximum difference in calculated attenuation factors (over distances considered) of about 2%. It justifies using the monoenergetic 1 MeV energy spectrum for all the samples considered.

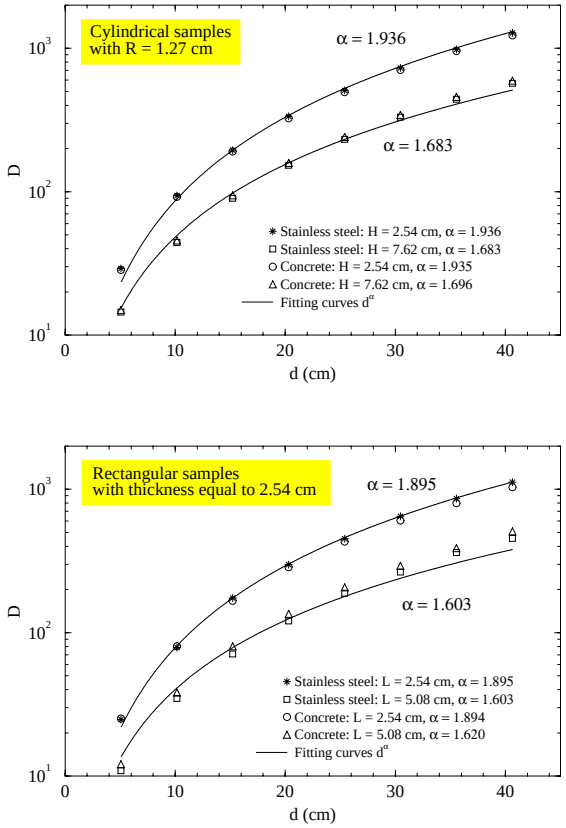

Fig. 3. Calculated surface dose rate attenuation factors, *D*, for cylindrical (top) and rectangular (bottom) samples *vs* distance from surface of sample, *d*.

IV. RESULTS AND DISCUSSION

IV.A. Residual dose rates

Comparison between measured and calculated residual dose rates for the samples near beam and above the steel shielding is presented in Figs. 4 through 6. In these Figures, the label FREDRON represents experimental data obtained by

[a] Such an option is used for coupling high- and low-energy parts in other codes as well.[10]

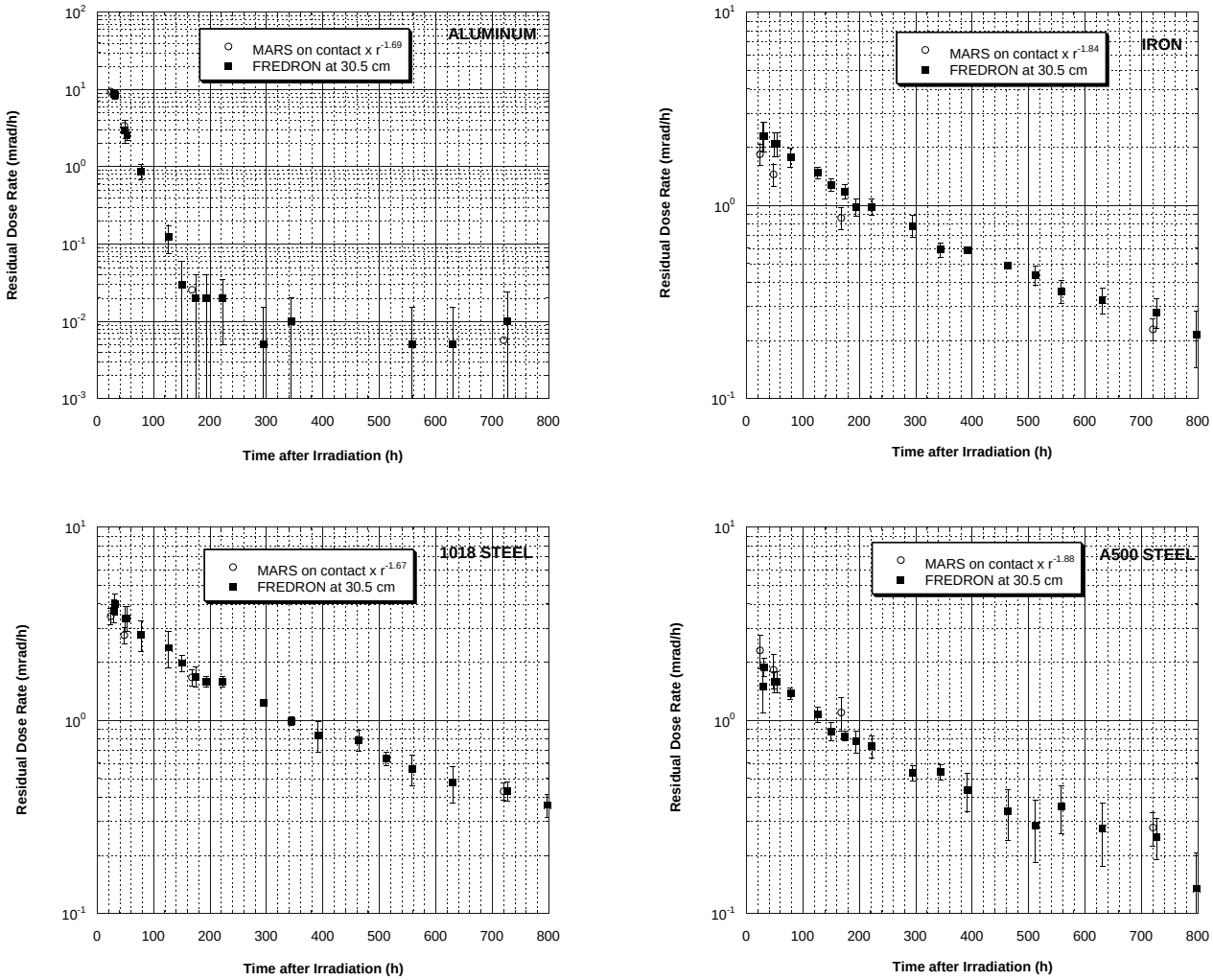

Fig. 4. Measured (FREDRON) and calculated (MARS) residual dose rate at $d = 30.5cm$ for the samples irradiated for 38 hours near beam *vs* cooling time.

means of the GM counter. In general, excellent agreement is observed for the near-beam irradiations (Figs. 4 and 6). The residual dose rates were calculated taking into account realistic non-continuous in time irradiation (three sessions, 16.2, 10.5, and 11 hours long, separated by different beam-off periods) as well as measured integrated proton intensities on the target. For above shielding irradiations (see Figs. 5 and 6), approximately 16 hours of beam-on was followed by 26 hours of beam-off on the average during the irradiation period of four months. That non-continuous irradiation was taken into account in our calculations as well. One can see that the agreement is good for aluminum and concrete samples and acceptable (i.e. within factors 2-3) for iron ones. The agreement between calculations and experiment is better for the near-beam location, in particular, because the ω-factors used were obtained from activation data in a cascade core. Another circumstance which influences quality of the results for the samples above the shielding is the necessity to consider the deep penetration problem which is not a trivial one itself.

Additional investigation has been performed for concrete samples (Fig. 6). According to our model, the calculated residual dose rate for the samples is very sensitive to the composition of the concrete. As an example, calculated residual dose rates above the steel shielding for different concrete sample compositions are shown in Table III. As observed, small differences in composition can lead to significant differences in calculated dose rates (up to a factor of 30). We attribute this effect mainly to minor admixtures in the region of Na (see Figs. 2 and 7). Most likely, this effect is due to the $^{23}\mathrm{Na}(n,\gamma)^{24}\mathrm{Na}$ reaction. Since we do not know exactly the

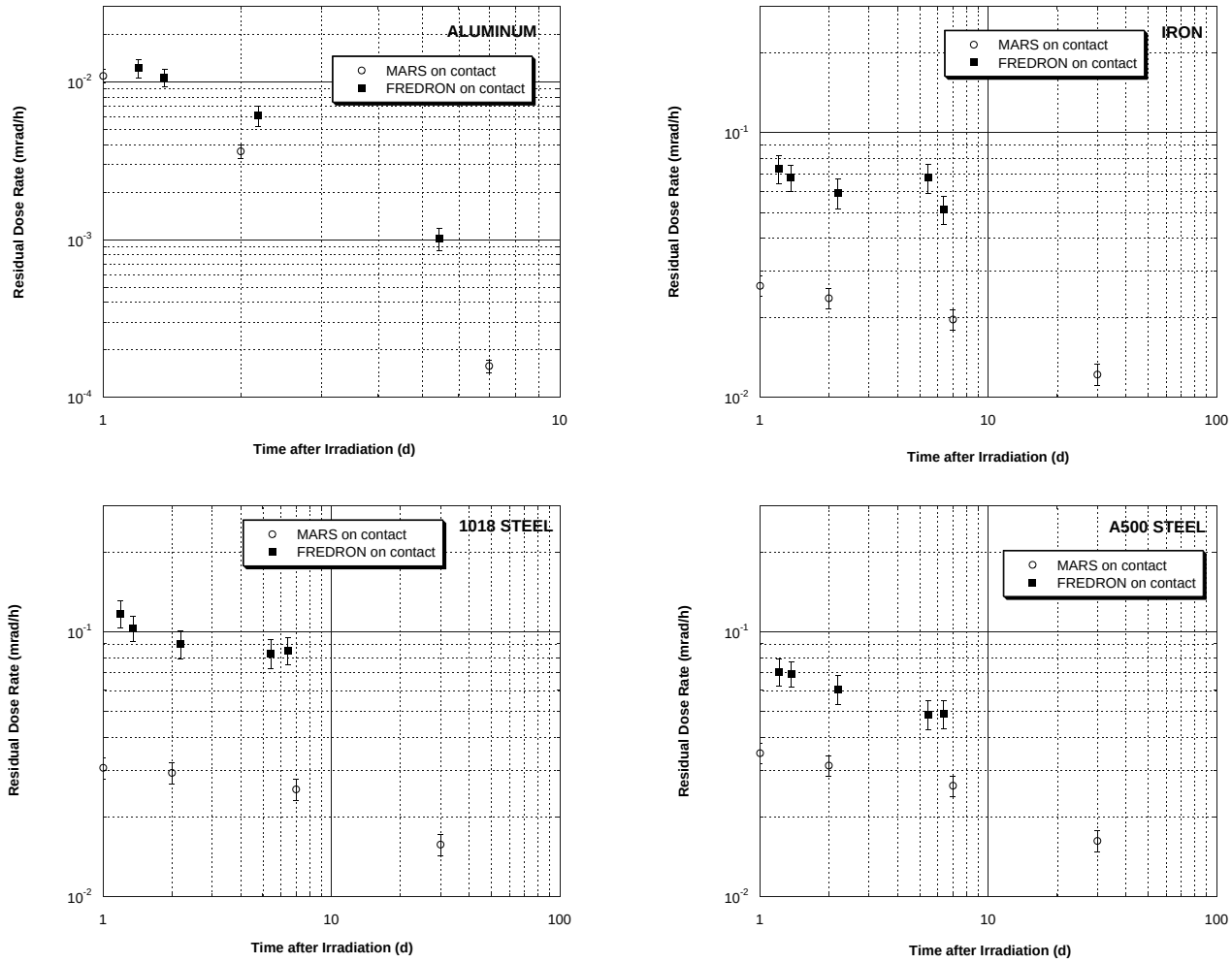

Fig. 5. Measured (FREDRON) and calculated (MARS) residual dose rate on contact for the samples irradiated for four months over the shielding *vs* cooling time.

composition of the concrete samples (with regard to minor admixtures) used in these studies, the discrepancy between calculations and measurements may not be unexpected.

IV.B. Neutron spectra

In the problem under investigation detailed neutron spectra at specific locations are of interest to get more insight into the problem and single out radiation which contributes significantly to calculated residual activity. Calculated neutron spectra near beam and above the shielding as well as the unfolded spectrum near beam based on measured foil activities are presented in Fig. 7. Location of the foils is shown in Fig. 1. Agreement between the calculated spectrum and unfolded (or, in other words, "measured") ones is quite good. One can see that even for the near-beam location the low-energy part of the neutron spectrum dominates, so that the contribution to observed residual activity from the low-energy particles should be taken into account. As for the spectrum above the vault shielding, the number of neutrons with energies above 20 MeV is well below one percent. However, their contribution to the residual dose rate is not negligible when compared to the other two neutron groups considered. In addition, one can see that in this location neutrons backscattered from the concrete walls and ceiling dominate (see Fig. 7). For the location above the shielding, therefore, one could not predict residual dose rates accurately without taking into account neutron backscattering from the concrete surroundings. In Table IV calculated partial residual dose rates for the samples are presented at fixed neutron flux and star density. The data can be useful to compare contributions to total residual dose rate from neutrons of different energy groups. Using the data from the Table along with calculated neutron flux and star density for the studied samples above the shielding, we find that for

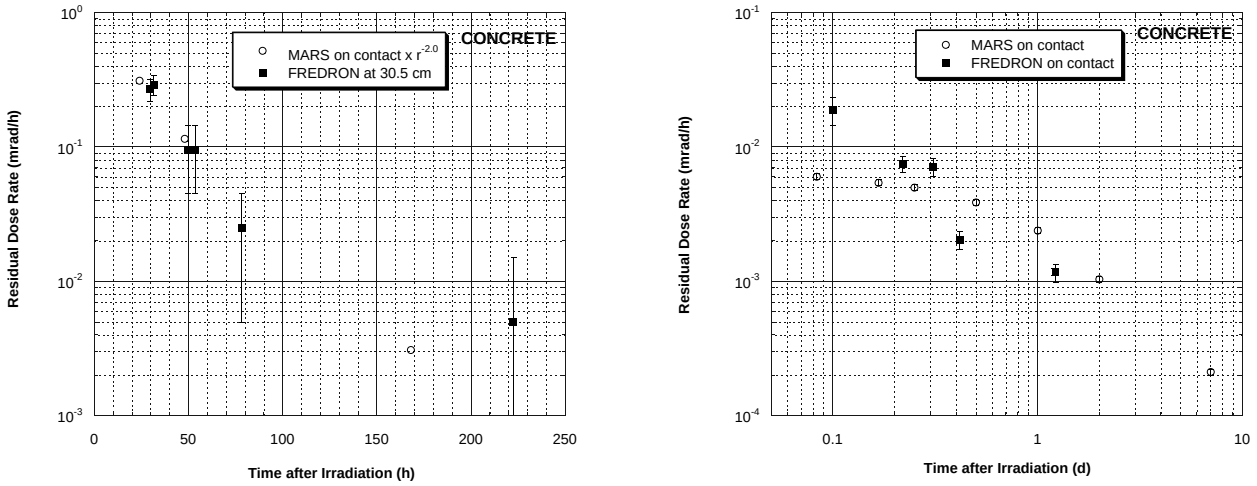

Fig. 6. Measured (FREDRON) and calculated (MARS) residual dose rate for the concrete samples irradiated for 38 hours near beam (left) and four months over the shielding (right) *vs* cooling time. The dose rates were measured at $d = 30.5cm$ and on contact, respectively. For the concrete samples the composition given as 3 in Table III was used in the calculations.

TABLE III. Calculated residual dose rates (10^{-4} mSv/h) for different compositions (weight %) of the concrete sample above the shielding. The data were obtained for 30 days irradiation at 10^{12} protons per second and 1 day cooling.

Concrete composition	Nuclide (or natural mixture)											Dose rate
	^{1}H	^{12}C	^{16}O	^{23}Na	Mg	^{27}Al	Si	S	K	Ca	Fe	
1	0.6		49.8	1.7	0.3	4.6	31.5		1.9	8.3	1.3	7.0
2	0.6	3.0	50.0	1.0		3.0	20.0		1.0	20.0	1.4	4.2
3	0.8	7.3	51.76	0.07	6.5	0.5	10.1	0.2	0.07	21.1	1.6	0.5
4	0.5	6.4	49.6		1.0	1.5	14.3	0.2		26.1	0.4	0.2

none of these samples is the partial residual dose rate induced by high energy neutrons ($E_n > 20$ MeV) dominating. For example, the contribution of this high energy group to total residual dose rate at 30 days irradiation and 1 day cooling for the aluminum, iron, and concrete samples equals to 12, 37, and 5%, respectively.

The neutron spectrum within the vault was unfolded from the measured radioactivity of Au and In foils. The response functions used in the unfolding codes BUNKI and LOUHI[3] were determined at eight rather broad energy bins in order to cover the neutron energy range up to 70 MeV. Therefore, at energies below 0.1 MeV, the unfolded spectrum represents a broad average, and this gives little quantitative information in comparison with the more detailed spectrum calculated with the MARS code. At energies above 0.1 MeV, however, acceptable agreement between calculations and measurements is observed, as seen in Fig. 7.

IV.C. Neutron streaming through air gaps

All the calculated results presented above were obtained with the presence of air gaps between the shielding modules and walls as well as between the modules themselves. In our model the gaps between the modules and walls on both sides were equal to 2.54 cm, while the four gaps between the modules themselves (see Fig. 1) were equal to 3.81, 1.42, 2.54, and 1.42 cm, respectively. To determine contribution to the activation above the shielding due to neutron streaming through the air gaps, calculations have been performed with all the gaps filled with the material of the shielding modules. Results of the calculations are presented in Fig. 8 and Table V. It should be noted that in this case neutron flux above 20 MeV was determined with high statistical uncertainty (about 50%).

V. CONCLUDING REMARKS

The model was developed for calculation of residual dose rates in arbitrary composite materials for arbitrary irradiation

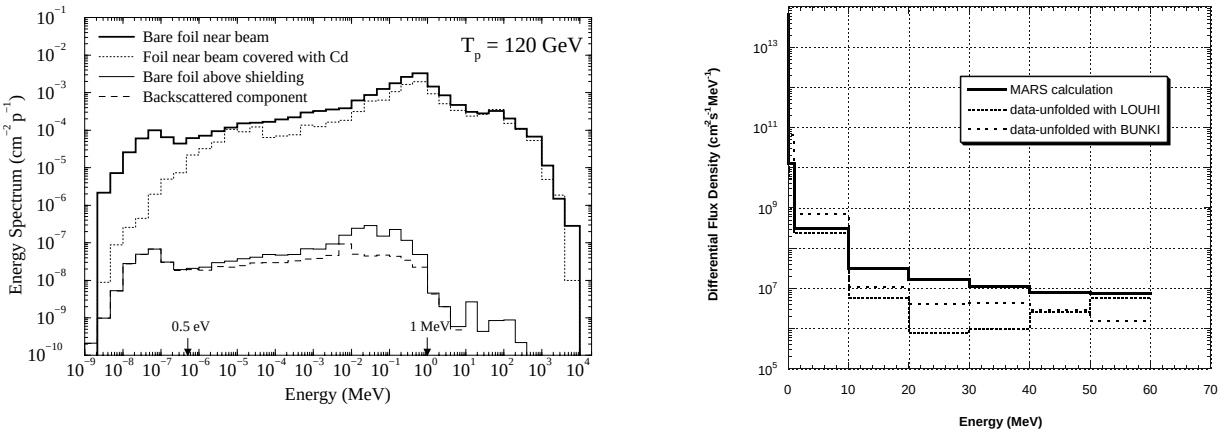

Fig. 7. Calculated neutron spectra (in units of n/cm^2 per energy bin and per proton) near beam and above the shielding (left) as well as unfolded spectra near beam (right). Normalization is per one incident proton (left) and 10^{12} protons per second (right).

TABLE IV. Calculated partial residual dose rates (mSv/h) for the samples described in Table I and irradiated with neutrons of the three energy groups. The data were obtained for one day cooling after 30 days irradiation at 1 star/cm^3·s in the first group and 1 n/cm^2·s in each of the other two groups.

Sample	Neutron energy (MeV)		
	Above 20	1-20	Below 5×10^{-7}
1 (Aluminum)	2.8×10^{-6}	1.2×10^{-7}	10^{-17}
2 (Iron)	3.1×10^{-6}	2.5×10^{-9}	6.1×10^{-9}
3 (1018 Steel)	3.1×10^{-6}	1.8×10^{-9}	5.3×10^{-9}
4 (Concrete)	8.2×10^{-7}	1.9×10^{-8}	4.8×10^{-9}
5 (A500 Steel)	3.1×10^{-6}	1.8×10^{-9}	6.2×10^{-9}

and cooling times. Measurements have been performed at FNAL on induced radioactivation of materials used for beam line components and shielding. Good agreement is observed between measured and calculated contact dose rates for different samples irradiated at different conditions, the agreement being better for the near-beam location because the ω-factors used were obtained from activation data in the cascade core. Calculated residual dose rate for the concrete sample above the shielding is very sensitive to the content of minor admixtures in concrete. When considering the activation above the shielding modules, contribution from neutron streaming through air gaps between the modules and walls as well as between the modules themselves is not negligible.

ACKNOWLEDGMENT

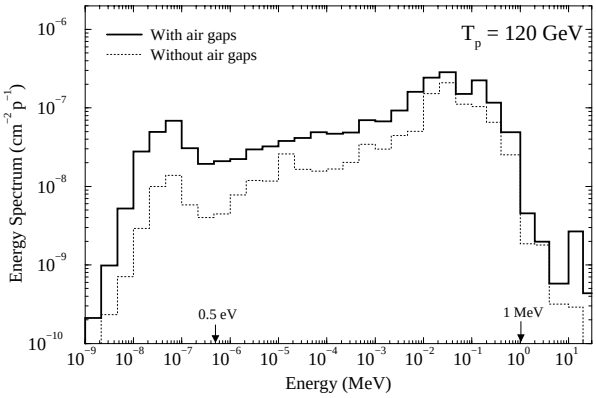

Fig. 8. Comparison between neutron spectra (in units of n/cm^2 per energy bin and per proton) calculated for the bare foil above the shielding with and without the presence of the air gaps between the shielding modules and walls as well as between the modules themselves. Normalization is per one incident proton.

We thank A. Wehmann and K. Vaziri of FNAL for helpful discussions on subjects covered in the paper.

REFERENCES

1. http://www-numi.fnal.gov:8875/
2. N. V. MOKHOV, "The MARS Code System User's Guide", Fermilab-FN-628 (1995); N. V. MOKHOV and O. E. KRIVOSHEEV, "MARS Code Status", Fermilab-Conf-00/181 (2000); http://www-ap.fnal.gov/MARS/.

TABLE V. Dose rate gap factors, *R*, for the samples (see Table I) above the shielding defined as the ratio of the residual dose rate calculated with the presence of the air gaps to that calculated without the gaps. The factors were obtained for 30 days irradiation and 1 day cooling. The uncertainties indicated represent one standard deviation (1σ).

Sample	R
1 (Aluminum)	2.6 ± 1.2
2 (Iron)	2.8 ± 0.5
3 (1018 Steel)	2.9 ± 0.6
4 (Concrete)	4.0 ± 0.5
5 (A500 Steel)	4.0 ± 0.6

3. K. LOWRY and T. JOHNSON, "Modification to Iterative Recursion Unfolding Algorithms and Computer Codes to Find More Appropriate Neutron Spectra", US Naval Research Laboratory, Report NRL-5340 (1984); J. T. ROUTTI and J. V. SANDEBERG, "General Purpose Unfolding LOUHI78 with Linear and Non-Linear Regularization", *Comp. Phys. Comm.*, **21**, 119 (1980).
4. P. AARNIO, *et al.*, CERN/TIS-RP/93-10; A. FASSÒ, *et al.*, *Proc. IV Int. Conf. on Calorimetry in High Energy Physics*, La Biodola, Sept 20-25, 1993, Ed. A. Menzione and A. Scribano, World Scientific, p. 493 (1993); A. FASSÒ, *et al., Proc. Specialists' Meeting on Shielding Aspects of Accelerators, Targets and Irradiation Facilities*, Arlington, Texas, April 28-29, 1994. NEA/OECD doc., p. 287 (1995).
5. W.B. WILSON, T.R. ENGLAND, K.A. VAN RIPER, "Status of CINDER90 Codes and Data", *Proc. IV SARE Workshop*, Knoxville, TN, September 1998, Ed. T.A. Gabriel, p. 69 (1998).
6. P.A. AARNIO, "Decay and Transmutation of Nuclides", CERN CMS NOTE–1998/086 (1998).
7. M. HUHTINEN, "Method for Estimating Dose Rates from Induced Radioactivity in Complicated Hadron Accelerator Geometries", CERN/TIS-RP/IR/98-28 (1998).
8. M. HUHTINEN and P. A. AARNIO, "Production of long-lived radionuclides in CMS", CERN CMS NOTE–1998/044 (1998).
9. J. F. BRIESMEISTER, editor, "MCNP - A General Monte Carlo N-Particle Transport Code", Version 4C. Pub. LA-13709-M, LANL (2000); http://www-xdiv.lanl.gov/XCI/PROJECTS/MCNP/.
10. R. E. PRAEL and H. LICHTENSTEIN, "User Guide to LCS: The LAHET Code System", Pub. LA-UR-89-3014, LANL (1989).